Nuclear Engineering and Technology 54 (2022) 1456–1463

Contents lists available at ScienceDirect

Nuclear Engineering and Technology

journal homepage: www.elsevier.com/locate/net

Original Article

Implementation of waste silicate glass into composition of ordinary cement for radiation shielding applications

Mohanad S. Eid [a], I.I. Bondouk [a], Hosam M. Saleh [b], Khaled M. Omar [a], M.I. Sayyed [c, d, *], Ahmed M. El-Khatib [e], Mohamed Elsafi [e, **]

[a] Physics Department, Faculty of Science, Tanta University, Tanta, Egypt
[b] Radioisotope Department, Nuclear Research Center, Egyptian Atomic Energy Authority, Egypt
[c] Department of Nuclear Medicine Research, Institute for Research and Medical Consultations (IRMC), Imam Abdulrahman Bin Faisal University (IAU), P.O. Box 1982, Dammam, 31441, Saudi Arabia
[d] Department of Physics, Faculty of Science, Isra University, Amman, Jordan
[e] Physics Department, Faculty of Science, Alexandria University, 21511, Alexandria, Egypt

ARTICLE INFO

Article history:
Received 17 July 2021
Received in revised form
6 October 2021
Accepted 7 October 2021
Available online 10 October 2021

Keywords:
Waste glass/cement
Geant4 simulation
MAC
Compressive
Porosity
Thermogravimetric analysis

ABSTRACT

The aim of this work is to study the radiation shielding properties of cement samples with waste glass incortated into its composition. The mass attenuation coefficient (MAC) of the samples were experimentally determined to evaluate their radiation shielding ability. The experimental coefficient was evaluated using NaI detector for gamma energies between 59.53 keV and 1408.01 keV using different radioactive point sources Am-241, Eu-152, Co-60, and Cs-137, and the gamma transmission parameters half-value layer, mean free path, and transmission factor were calculated. The theoretical coefficient of the composites was determined using Geant4 and XCOM software. The results were also compared against Geant4 and XCOM simulations by calculating the relative deviation between the values to determine the accuracy of the results. In addition the mechanical properties (including Compressive and porosity) as well as the thermogravimetric analysis were tested for the present samples. Overall, it was concluded that the cement sample with 50% waste glass has the greatest shielding potential for radiation shielding applications and is a useful way to reuse waste glass.

1. Introduction

Over the past century, the number of technologies that utilize radiation to function has drastically increased due to the advancements in fields such as energy generation and medicine. Radiation offers many benefits, such as an alternative power source to fossil fuels; however, radiation leaks remain a concern and must be effectively managed to avoid potential harm to humans and the environment. Due to the nature of ionizing radiation, or radiation with sufficient energy to detach electrons from atoms, exposure to these types of photons can lead to permanent long-term damage to the human body. To avoid these effects, radiation shields are used to protect workers and patients from the incoming photons [1–5].

Depending on the energy, particle type, and application, different radiation shields are more effective in certain circumstances. One of the main types of radiation shields commonly used are concretes [6,7]. Concretes are versatile in nature and are not toxic, unlike lead, which is widely used, while having an excellent resistance to water, is easily modifiable, has a low cost, requires low maintenance, and can be easily manufactured around the world. They can be used to line the walls of nuclear power plants, X-ray rooms, and particle accelerators. By introducing different components into the composition of concretes, new shields have been developed such as self-curing concrete and self-compacting concretes. Additionally, glass can be incorporated into concretes to improve the properties of the shield [8–10].

To achieve the sustainability, various types of waste or undesired additives have been added to cement for proper nuclear protection applications such as micro-cellulose [11], natural clay [12,13], plant wastes [14], plastic waste [15,16], wastes generated during cement manufacturing [17].

* Corresponding author. Department of physics, Faculty of Science, Isra University, Amman, Jordan.
** Corresponding author.
E-mail addresses: dr.mabualssayed@gmail.com (M.I. Sayyed), mohamedelsadi68@gmail.com (M. Elsafi).

https://doi.org/10.1016/j.net.2021.10.007

Glass waste has become an increasingly large problem throughout the world due to the increase in the consumption of materials. Although recycling technologies have allowed the complete reuse of used glass, an extremely high amount of waste glass still ends up in landfills. Furthermore, some types of glasses, such as Pyrex and borosilicate glass, are not considered recyclable, and simply get thrown out. Additionally, since different glasses have varying melting points, mixing glasses could result in a glass mixture with a different viscosity and could cause cracking and shattering. Therefore, by incorporating waste glass into the composition of cement, the problem of unusable glass can be resolved, while improving the shielding ability of the cement at the same time [18–20].

Since glass contains high amounts of silica (around 72%), it can be finely pulverized and combined with cement to improve the structural properties of the cement while minimizing CO_2 emotions. Reusing glass also reduces waste and saves more natural resources. Other characteristics such as flexibility and tensile strength have also been analyzed. Moreover, previous studies have attempted to combine large quantities of waste glass to create polymeric glass composite panels. Glasses have been used for fillers in the asphalt, pavements, and sidewalk slabs as additions to cement and concrete. Waste glass is often used in the construction of materials as a substitute to other ingredients [21–23]. Therefore, the aim of this study is to enhance the shielding property of the cement at the same time produce a sustainable product that makes use of the waste into useful products by analyzing the mechanical, thermal, porosity, and radiation shielding properties of ordinary cement with waste glass powder incorporated in its composition.

2. Material and methods

2.1. Preparation of samples

Two different materials were utilized in this study. The first was Ordinary Portland cement (CEMI 42.5 N), which was manufactured locally by Suez Cement, an Egyptian company, and meets the requirements of Egyptian standards ES 4756/1–2013 and obeys the European specifications EN 197/1–2011. Additionally, glass with high silicate contents acquired from broken waste glass equipment's (mainly beakers and test tube) was grinded until it became fine powder that was easy to handle. In the present study, six series of mortar mixtures were prepared. In each series six samples were elected. There were used in measuring the compressive strength values and the other three were used in the density and porosity measurement; the rest of the samples were used to determine the gamma attenuation coefficient.

To prepare the mortal samples with various compositions we used the next formula:

Cement + glass waste + adequate tap water (70%)

Starting with 0%–50% glass waste and a constant ratio of water, which is 35% relative to the total weight of the mixture, the mixture was robustly shaken to obtain a homogeneous mortar paste. This paste was then casted into the desired cylindrical shape by pouring it in cylindrical plastic molds with the same volume after filling the interior surface with an oily substance to avoid the mortar sticking to the mold. The poured mortal mixture is then stored at room temperature (24 ± 3° Celsius) for a complete reaction with water, and for the setting and hardening to complete. After 28 days, the water was dried out from the samples and became a rigid solid, as shown in Fig. 1. The samples were then taken to carry out the above mentioned tests along with the spectroscopic analyses.

2.2. Compressive strength test and porosity measurement

A hydraulic presser was used to evaluate the compressive strength for at least 3 samples from each series, according to the technique of the examined ASTM conditions [24]. Using Archimedes' saturation technique, the water displacement method can be used to measure the mass of porous samples both dry and submerged in water. Bulk density and the apparent porosity **P** of the samples can be determined according to previous literatures [25,26]. The compressive strength and the porosity were calculated and graphed in Fig. 2.

2.3. Sample characterization

The chemical compositions of the glass/cement samples were determined by using the Energy-Dispersive-X-ray analysis (EDX)

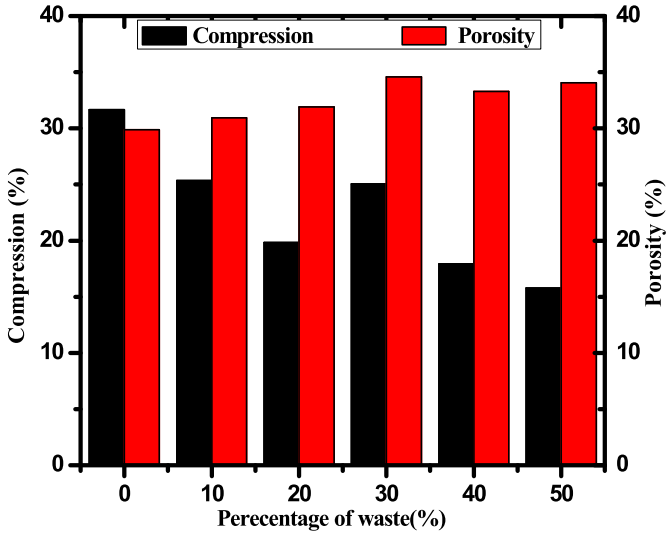

Fig. 2. The compressive strength and the porosity as a function of waste glass percentages mixed with the cement.

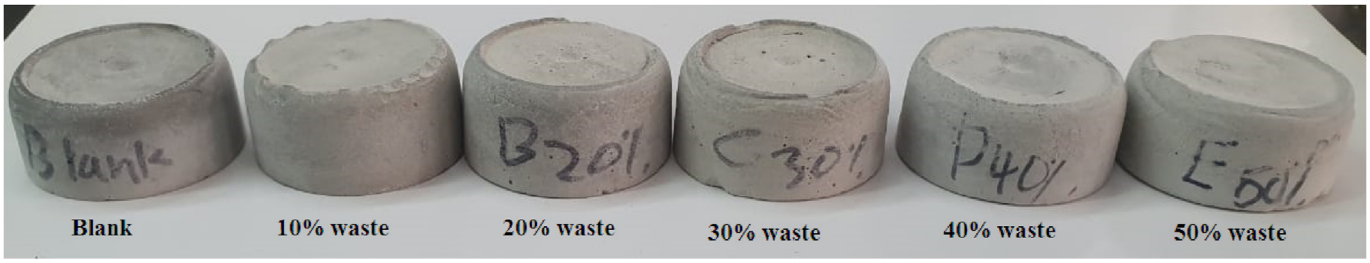

Fig. 1. The prepared samples used in the present work.

Table 1
Chemical composition of waste glass/cement samples after preparation using EDX.

Elements	10% waste/cement (ρ = 1.67 g/cm^3)	20% waste/cement (ρ = 1.68 g/cm^3)	30% waste/cement (ρ = 1.72 g/cm^3)	40% waste/cement (ρ = 1.80 g/cm^3)	50% waste/cement (ρ = 1.81 g/cm^3)
O	0.5310	0.5380	0.5470	0.5518	0.5588
Mg	0.0100	0.0089	0.0078	0.0067	0.0056
Al	0.0223	0.0219	0.0222	0.0224	0.0227
Si	0.0999	0.1306	0.1614	0.1921	0.2229
S	0.0102	0.0100	0.0079	0.0068	0.0057
Ca	0.2964	0.2634	0.2305	0.2000	0.1680
Fe	0.0208	0.0185	0.0162	0.0139	0.0116
ZnO	0.0095	0.0085	0.0074	0.0064	0.0053
Na	0.0044	0.0089	0.0133	0.0178	0.0222
Total	1.0000	1.0000	1.0000	1.0000	1.0000

unit of a scanning electron microscope. The glass/cement compositions and their densities are tabulated in Table .1. The glass/cement samples were also examined using a scanning electron microscope to assess the homogenous distribution of waste glass in cement.

Fourier Transform Infrared (FT-IR) spectroscopy was used to test the present samples (Fig. 3) and the results show the presence of portlandite ($Ca(OH)_2$), which is well detected by unique peaks around 3640 cm^{-1} in all the samples, which is due to the stretching vibration of the hydroxyl group. Furthermore, cementation materials characterized by peaks between 975 cm^{-1} and 1000 cm^{-1} indicate the presence of Calcium Silicate Hydrate (C–S–H), which is due to the Si–O asymmetric stretching vibration. The peaks at 713 cm^{-1},875 cm^{-1} and 1440 cm^{-1} indicate the presence of different vibration modes of the carbonate group. Peaks at 1640 cm^{-1} and 3440 cm^{-1} indicate the vibration of the O–H group of capillary water. The peak at 1110 cm^{-1} corresponds to sulfate, while the silicate in the glass waste is represented by the peaks at 460 cm^{-1}, which increase when increasing the amount of glass added to the cement.

Four of the present samples were subjected to thermogravimetric analysis (TGA). The samples were heated from room temperature to 840 °C in a PerkinElmer thermo analyzer at a heating rate of 10 °C min^{-1}. Reduction in the total weight loss was noticed as the ratio of waste glass increased in the glass/cement composites, as shown in Fig. 4. The percentage of the total weight losses due to heating from 28 °C to 840 °C were between 27.47% for the 0% sample to 20.78% for the 50% sample.

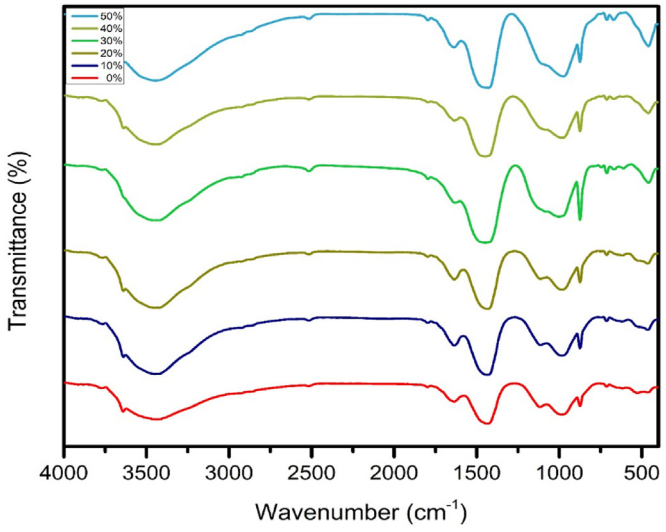

Fig. 3. The FT-IR properties to show the transmittance of different samples discussed as a function of the wave number.

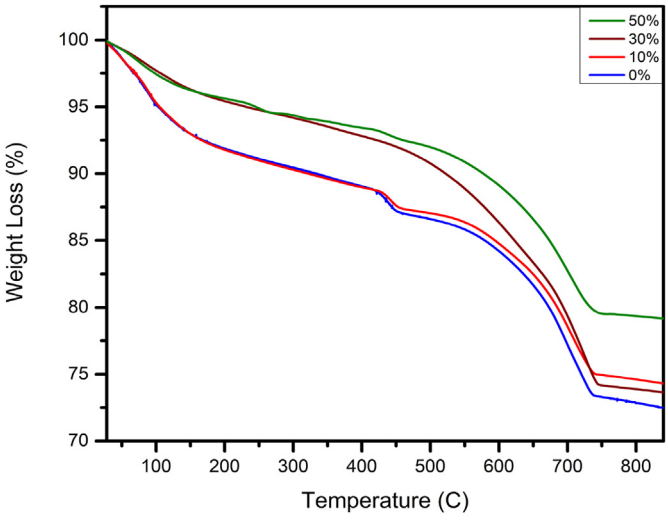

Fig. 4. The percentage of weight loss of the present samples as a function of temperature.

2.4. Shielding parameter calculations

The MAC was experimentally determined using a NaI scintillation detector and different radioactive point sources to cover the range of different energies. The experimental setup technique is shown in Fig. 5 and the specification of the point source used in the present work is tabulated in Table.2 [27,28]. The MAC can be determined from the well-known Beer-Lambert's law [29] as follows:

$$MAC = \frac{1}{x.\rho}\ln\left(\frac{I_0}{I}\right) \quad (1)$$

where I_0 and I are the incident and transmitted intensities, respectively, passing through a target material of thickness x, and ρ is the density of the measured sample. The intensity of the gamma ray line represents the count rate or the peak area per unit time, which were analyzed using the Genie 2000 software. Also, by knowing the initial and transmitted intensities, the transmission factor TF can experimentally be calculated at varying sample thicknesses.

The LAC is affected by the density of the absorber, so to calculate the LAC, the MAC must be multiplied by the density of the measured sample. The HVL is the thickness needed to reduce the intensity of the incoming photons by 50% and its equation is the following [30]:

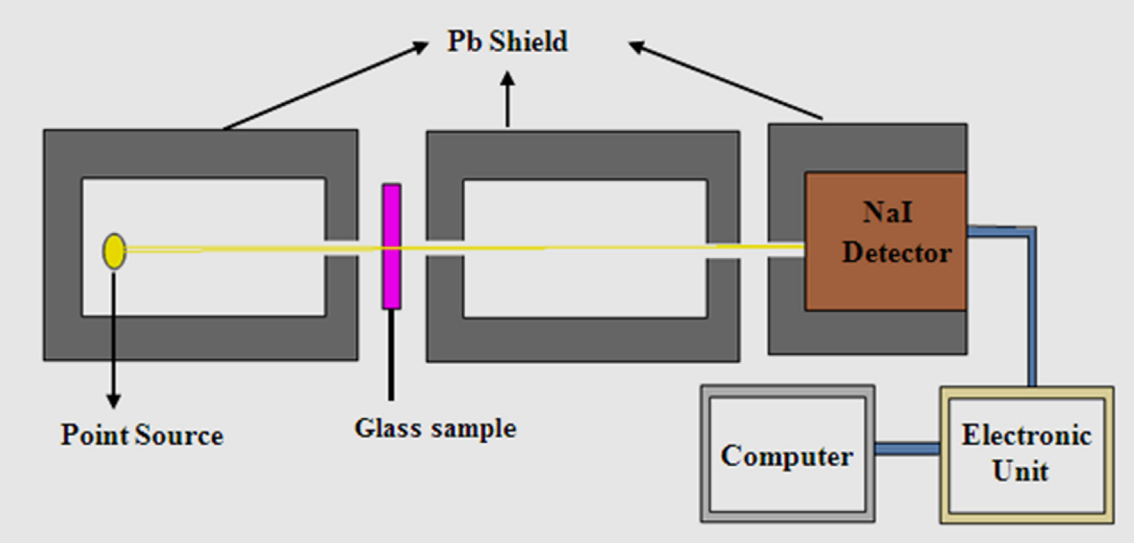

Fig. 5. The schematic diagram of experimental setup of narrow beam method.

Table 2
The activities and other specifications for point sources which are used in the present study with reference date 1/1/2009.

Nuclide	Energy keV	Activity Bq	Uncertainty kBq	Emission Probability
Am-241	0.0595	259000	±2.6	35.9
Cs-137	0.6617	385000	±4.0	34.1
Eu-152	0.1216	290000	±4.0	28.4
	0.2447			26.6
	0.3443			14
	0.9641			20.87
	1.4081			85.21
Co-60	1.1733	212100	±1.5	99.9
	1.3327			99.982

$$HVL = \frac{\ln 2}{LAC} \tag{2}$$

The mean free path MFP is the average distance which a photon travels between two successive interactions and is described by the following equation [31]:

$$MFP = \frac{1}{LAC} \tag{3}$$

2.5. Geant4 code

The current work was studied by using Geant4 code (version 10.3.P3). Geant4 is a universal Monte Carlo simulation that can be utilized to study the history of electrons, protons, and neutrons or a coupling between them inside the medium [32,33]. The setup of the experimental work was simulated, as well as the chemical composition of each sample. The simulation was analyzed to obtain the net area under the peak using ROOT software [34]. The simulation was run with the presence and absence of the glass sample to obtain the peak area within and without the glass sample, taking into account that the primary photons are fixed at both cases. In all simulations, at least 10^7 primary monoenergetic photons must be generated to get the lowest possible relative error [35]. The area under each calculated peak represents the intensity of this line, so the mass-attenuation coefficient can be calculated using Geant4 code according Beer-Lambert's law.

3. Results and discussion

The experimental and Geant4 mass attenuation coefficients for the prepared cement samples with waste glasses were determined and listed in Table 3. Moreover, the relative deviation between the experimental and Geant4 MAC for the prepared cement samples with waste glasses were determined and graphed in Fig. 6. First, this figure demonstrates that all the values are within a ±3%

Table 3
The experimental and Geant4 mass attenuation coefficients for the prepared cement samples with waste glasses.

Energy (MeV)	Blank		10%		20%		30%		40%		50%	
	Exp	Geant4	Exp	Geant4	Exp	Geant4	Exp	Geant4	Exp	Geant4	Exp	Geant4
5.95E-02	0.6476	0.6590	0.6456	0.6424	0.6085	0.6225	0.6002	0.6123	0.5975	0.6054	0.5820	0.5896
1.22E-01	0.2806	0.2779	0.2834	0.2802	0.2854	0.2816	0.2871	0.2848	0.2933	0.2911	0.2958	0.2926
2.45E-01	0.1971	0.1947	0.1919	0.1978	0.2004	0.1999	0.2031	0.2031	0.2114	0.2104	0.2132	0.2138
3.44E-01	0.1699	0.1680	0.1694	0.1717	0.1749	0.1722	0.1776	0.1773	0.1829	0.1827	0.1864	0.1857
6.62E-01	0.1242	0.1263	0.1280	0.1295	0.1265	0.1304	0.1310	0.1332	0.1363	0.1379	0.1379	0.1404
7.79E-01	0.1188	0.1180	0.1210	0.1192	0.1230	0.1220	0.1255	0.1245	0.1297	0.1289	0.1320	0.1308
9.64E-01	0.1045	0.1070	0.1096	0.1083	0.1105	0.1099	0.1123	0.1126	0.1158	0.1165	0.1181	0.1184
1.17E+00	0.0947	0.0959	0.0988	0.0986	0.0987	0.0996	0.1015	0.1019	0.1046	0.1052	0.1064	0.1070
1.33E+00	0.0916	0.0903	0.0919	0.0926	0.0943	0.0928	0.0961	0.0953	0.0992	0.0985	0.1011	0.1003
1.41E+00	0.0866	0.0875	0.0875	0.0891	0.0881	0.0907	0.0907	0.0923	0.0942	0.0957	0.0955	0.0973

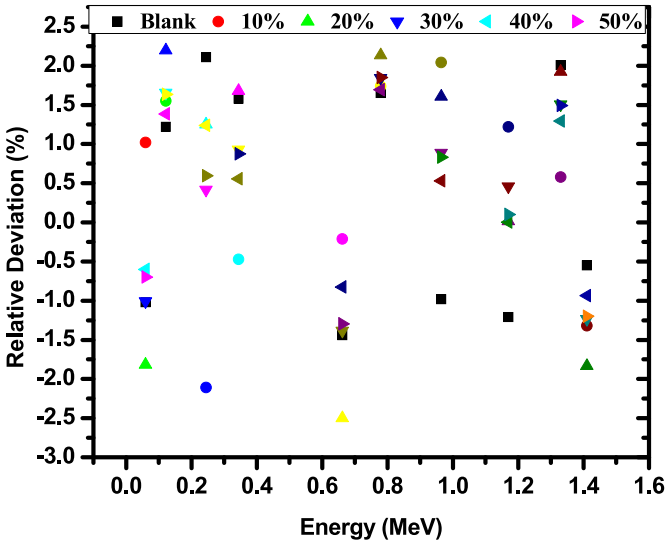

Fig. 6. Relative deviation between the experimental and Geant4 values for the mass attenuation coefficient.

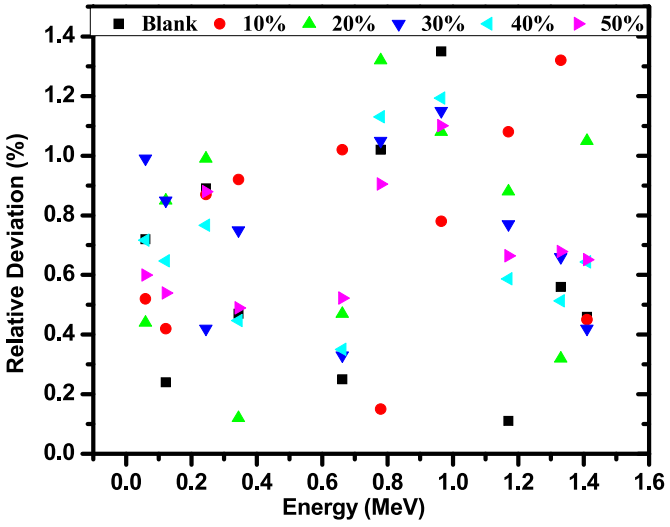

Fig. 7. Relative deviation between the XCOM and Geant4 values for the mass attenuation coefficient.

deviation, which proves the accuracy and precision of the experimental results used to obtain the MAC values. For example, the sample coded as 20% had an MAC value at 0.344 MeV equal to 0.1749 cm^2/g obtained experimentally and 0.1722 cm^2/g obtained from Geant4. Meanwhile, at 1.17 MeV, the MAC values are equal to 0.0987 cm^2/g and 0.0996 cm^2/g for the same respective methods. No observal trend could be seen between deviation and energy or waste glass content.

Additionally, Fig. 7 demonstrates the relative deviation between the MAC values obtained from XCOM and Geant4 to compare the two approaches. In this figure, all values have an even smaller deviation than the previous figure (all within 1.5%). This result indicates that both methods are in extremely good agreement with each other, and reaffirms the reliability of the results. Once again, no observable trend could be seen between the relative deviation and energy or relative deviation and waste glass content.

The linear attenuation coefficient (LAC) of the cement samples was graphed against increasing energy in Fig. 8. As a general trend,

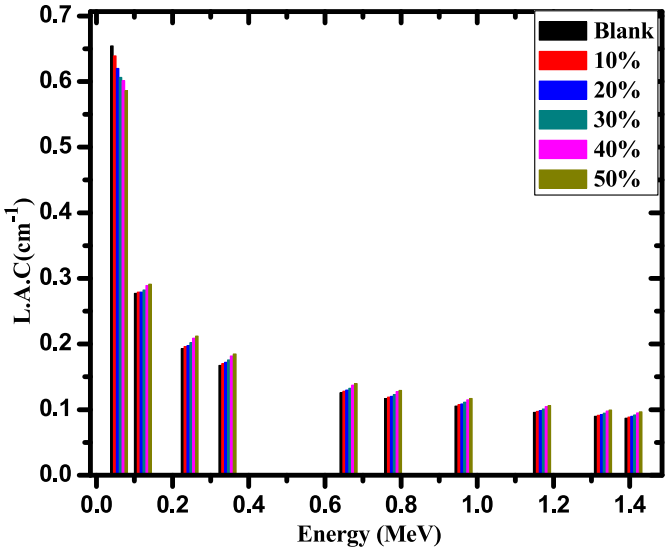

Fig. 8. The linear attenuation coefficient for the fabricated cement with different amount of waste glasses.

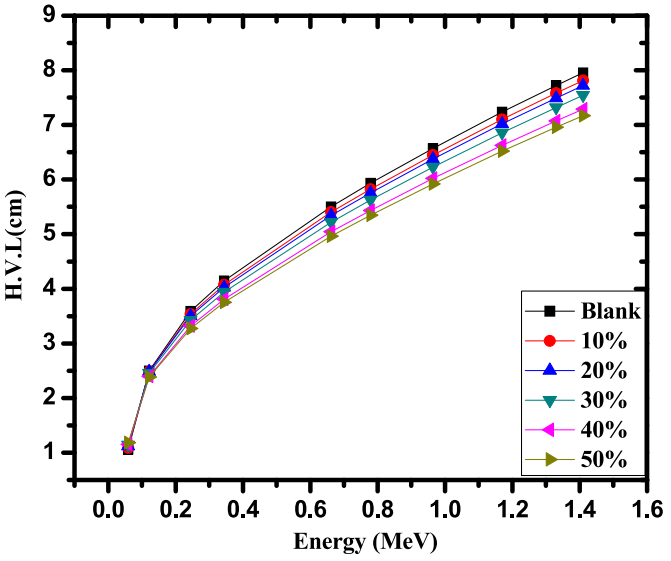

Fig. 9. The half value layer for the fabricated cement with different amount of waste glasses.

the LAC values decrease with increasing energy due to the increased penetration power of high energy photons. For instance, the LAC of the sample coded as 20% decreases from 0.620 cm^{-1} at 0.0595 MeV to 0.198 cm^{-1} at 0.245 MeV, 0.130 cm^{-1} at 0.662 MeV, 0.0987 cm^{-1} at 1.17 MeV, and 0.0898 cm^{-1} at 1.41 MeV. The LAC results can also be compared against each other at a single energy. At all energies except 0.0592 MeV, the LAC values follow the order of Blank <10% < 20% < 30% < 40% < 50%. For example, at 0.964 MeV, the LAC values are equal to 0.106, 0.107, 0.109, 0.111, 0.115, and 0.117 cm^{-1} for the samples coded as Blank, 10%, 20%, 30%, 40%, and 50%, respectively. This trend is expected as the cement with 50% waste glass has a greater density than the other samples, and since LAC is a density dependent parameter, it is natural that this sample has the greatest LAC. Therefore, at most tested energies, the fabricated cement sample with 50% waste glass has the best shielding ability out of the tested samples.

Half value layer, or HVL, represents the thickness of a sample

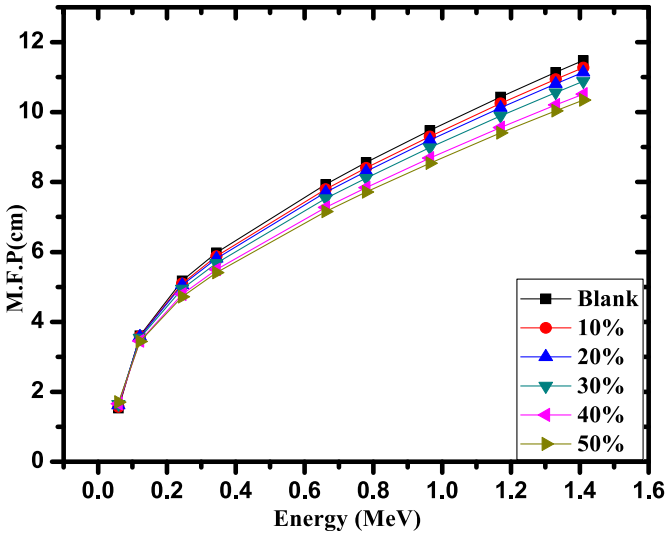

Fig. 10. The mean free path for the fabricated cement with different amount of waste glasses.

needed to reduce the intensity of the incoming radiation to half of its original value [36–38]. Due to the nature of its definition and its inverse relation with LAC, a smaller HVL means a thinner, and thus a better shield. The HVL of the fabricated samples was graphed as a function of increasing energy in Fig. 9. For all the tested samples, HVL increases with increasing energy. For example, the HVL of the cement with 10% waste glass increases from 1.08 cm to 7.81 cm at energies equal to 0.0595 MeV and 1.41 MeV, respectively, while the HVL of the cement with 40% waste glass increases from 1.15 cm to 7.29 cm for the same respective energies. This trend occurs because higher energy photons have an easier time penetrating through the sample, so a thicker shield is needed to attenuate the same amount of radiation. This result therefore means that the cement is more space-efficient against lower energy photons, and must be thicker to provide the same amount of safe protection against higher energy photons. From this figure, the HVL of the cement samples can also be compared against each other. At all energies, but especially at high energies, the cement sample with 50% waste glass has the lowest HVL, while the cement with no waste glass has the greatest, meaning that the former is the most space-efficient, while the latter is the least. At 0.122 MeV, for example, the cement with no waste glass has an HVL equal to 2.50 cm, while the cement with 50% waste glass an HVL equal to 2.38 cm. Thus, it can also be concluded from this figure that the cement with 50% waste glass has the greatest shielding potential out of the investigated glasses.

Fig. 10 demonstrates the mean free path (MFP) of the tested samples against incoming photon energy [39–41]. MFP is the reciprocal of LAC and is defined as the distance between subsequent collisions. Thus, a lower MFP represents more collisions, more attenuation, and a better shield. The MFP of the cement samples increases with increasing energy. For example, the MFP of the concrete samples with 30% waste glass increases from 1.65 cm at 0.595 MeV to 5.05 cm at 0.245 MeV, 7.71 cm at 0.662 MeV, 10.1 cm at 1.17 MeV, and 11.1 cm at 1.41 MeV. This increasing trend occurs because higher energy photons tend to interact with the incident material less often, reducing the number of collisions and increasing the distance between collisions, or MFP. This result indicates that the samples, perform better against lower energy photons, which is expected. Additionally, it can be seen that the concrete with 50% waste glass has the lowest MFP at all energies, while the blank concrete has the greatest MFP. This result agrees with the data obtained from the HVL values.

Fig. 11[a-d] illustrate the transmission factor (TF), sometimes referred to as the transmission rate, of the cement with no waste glass, 20% waste glass, and 50% waste glass against increasing thickness at four selected energies. TF represents the percentage of photons that transmit through a sample, meaning that a lower TF means a greater shielding ability. At all four energies TF decreases with increasing thickness. When observing subfigure [a] by itself, for example, the TF of the cement with 20% waste glass decreases from 0.538% to 0.290%, 0.045%, and 0.002% for thicknesses of 1, 2, 5, and 10 cm, respectively. As can be seen from these values, TF drastically decreases with increasing thickness. This result means that increasing the thickness of the cement samples drastically improves their shielding abilities. The TF of the samples can also be compared against each other at a single energy and thickness. In these conditions, the TF values follow the order of 50% < 20% < cement. At an energy of 0.6616 MeV and a thickness of 5 cm, the TF values are equal to 0.533%, 0.523%, and 0.497% for the cement, 20%, and 50% samples, respectively. This result indicates that the cement sample with 50% waste glass has the best shielding ability, as it has the lowest TF at all thicknesses. Lastly, another trend can be observed when comparing the subfigures against each other. In this case, or as energy increases for a single thickness, the TF values increase. This occurs because higher energy photons have an easier time penetrating through absorber materials, increasing TF. Overall, it can be concluded that the samples are most effective at low energies and high thicknesses, and that the cement sample with 50% waste glass is the most effective out of the investigated samples.

4. Conclusion

This study analyzed the effect of adding waste glass to cement to its radiation shielding properties to find a useful means to reuse this material. The study experimentally determined the MAC, LAC, HVL, MFP, and TF of the samples to determine the shielding ability of these cements. Additionally, by comparing the experimental values to the theoretical results obtained through XCOM and Geant4, it was found that all three methods strongly agree with each other. The LAC results revealed that the cement samples with 50% waste glass had the best shielding ability at most energies, as it had the greatest LAC, while the sample with no waste glass had the least. More specifically, the LAC values followed the order of Blank <10% < 20% < 30% < 40% < 50%. Furthermore, the HVL and MFP of the samples showed that the shielding ability of the samples decreased with increasing energy, as higher energy photons cause the shielding to become less effective. These parameters also revealed that the sample coded as 50% had the most desirable parameters when comparing the tested samples against each other. Next, the TF of the cements showed that increasing the thickness of the shields improves their attenuation capability, as less photons are able to penetrate through the samples. Altogether, it was concluded that the cement sample with 50% waste glass had the best shielding ability for radiation shielding appliactons and that

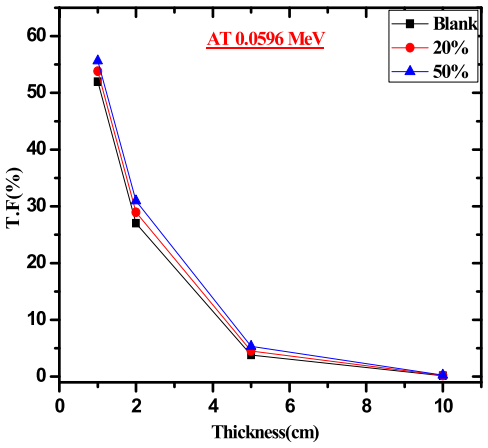

a: The tranmssion factor for the fabricated cement with different amount of waste glasses at 0.0596 MeV

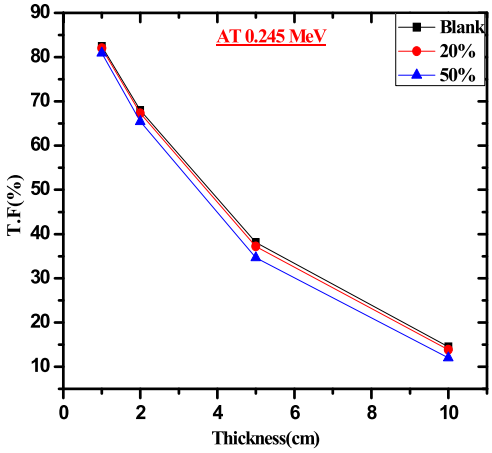

b: The tranmssion factor for the fabricated cement with different amount of waste glasses at 0.245 MeV

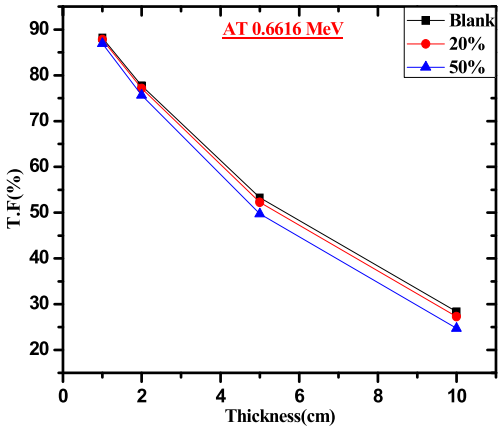

c: The tranmssion factor for the fabricated cement with different amount of waste glasses at 0.6616 MeV

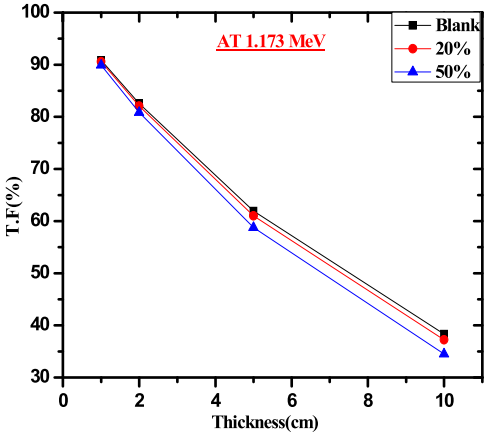

d: The tranmssion factor for the fabricated cement with different amount of waste glasses at 1.173 MeV

Fig. 11. a: The tranmssion factor for the fabricated cement with different amount of waste glasses at 0.0596 MeV
Fig.11-b: The tranmssion factor for the fabricated cement with different amount of waste glasses at 0.245 MeV
Fig.11-c: The tranmssion factor for the fabricated cement with different amount of waste glasses at 0.6616 MeV
Fig.11-d: The tranmssion factor for the fabricated cement with different amount of waste glasses at 1.173 MeV.

incoprotaing waste glass into cement is a useful way to reuse these materials.

Declaration of competing interest

The authors declare that they have no known competing financial interests or personal relationships that could have appeared to influence the work reported in this paper.

References

[1] Y.S. Rammah, K.A. Mahmoud, M.I. Sayyed, F.I. El-Agawany, R. El-Mallawany, Novel vanadyl lead-phosphate glasses: P2O5–PbO–ZnONa2O–V2O5: synthesis, optical, physical and gamma photon attenuation properties, J. Non-Cryst. Solids 534 (2020) 119944.

[2] M. Dong, S. Zhou, X. Xue, X. Feng, M.I. Sayyed, M.U. Khandaker, D.A. Bradley, The potential use of boron containing resources for protection against nuclear radiation, Radiat. Phys. Chem. (2021) 109601.

[3] M.I. Sayyed, Y. Al-Hadeethi, M.M. AlShammari, M. Ahmed, S.H. Al-Heniti, Y.S. Rammah, Physical, optical and gamma radiation shielding competence of newly boro-tellurite based glasses: TeO2–B2O3–ZnO–Li2O3–Bi2O3, Ceram. Int. 47 (2021) 611–618.

[4] M.I. sayyed, Y. Elmahroug, B.O. Elbashir, Shams A.M. Issa, Gamma-ray shielding properties of zinc oxide soda lime silica glasses, J. Mater. Sci. Mater 28 (2017) 4064–4074.

[5] M. Elsafi, M.F. Alrashedi, M.I. Sayyed, I.F. Al-Hamarneh, M.A. El-Nahal, M. El-Khatib, M.U. Khandaker, H. Osman, A.E. Askary, The potentials of Egyptian and Indian granites for protection of ionizing radiation, Materials 14 (2021) 3928, https://doi.org/10.3390/ma14143928.

[6] B. Aygün, E. Şakar, O. Agar, M.I. Sayyed, A. Karabulut, V.P. Singh, Development of new heavy concretes containing chrome-ore for nuclear radiation shielding applications, Prog. Nucl. Energy 133 (2021) 103645.

[7] K.A. Mahmoud, M.I. Sayyed, O.L. Tashlykov, Comparative studies between the

shielding parameters of concretes with different additive aggregates using MCNP-5 simulation code, Radiat. Phys. Chem. 165 (2019) 108426.
[8] G. Tyagi, A. Singhal, S. Routroy, D. Bhunia, M. Lahoti, A review on sustainable utilization of industrial wastes in radiation shielding concrete, Mater. Today Proc. 32 (2020) 746–751.
[9] Y.S. Choi, S.M. Lee, Fundamental properties and radioactivity shielding performance of concrete recycled cathode ray tube waste glasses and electric arc furnace slag as aggregates, Prog. Nucl. Energy 133 (2021) 103649.
[10] F. Pahlevani, V. Sahajwalla, From waste glass to building materials–An innovative sustainable solution for waste glass, J. Clean. Prod. 191 (2018) 192–206.
[11] M.M.A. Dawoud, M.M. Hegazy, W.K. Helew, H.M. Saleh, Overview of environmental pollution and clean management of heavy metals and radionuclides by using microcrystalline cellulose, J. Nucl. Ene. Sci. Power Gener. Technol 3 (2021) 2.
[12] T.A. Bayoumi, H.M. Saleh, S.B. Eskander, Solidification of hot real radioactive liquid scintillator waste using cement–clay composite, Monatshefte Für Chemie-Chemical Mon 144 (2013) 1751–1758.
[13] H.M. Saleh, Some applications of clays in radioactive waste management, in: L.R. Wesley (Ed.), Clays Clay Miner. Geol. Orig. Mech. Prop. Ind. Appl., Nova Science Pub. Inc, 2014, pp. 403–415.
[14] H.M. Saleh, R.F. Aglan, H.H. Mahmoud, Qualification of corroborated real phytoremediated radioactive wastes under leaching and other weathering parameters, Prog. Nucl. Energy. 119 (2020) 103178, https://doi.org/10.1016/j.pnucene.2019.103178.
[15] S.B. Eskander, H.M. Saleh, M.E. Tawfik, T.A. Bayoumi, Towards potential applications of cement-polymer composites based on recycled polystyrene foam wastes on construction fields: Impact of exposure to water ecologies, Case Stud. Constr. Mater 15 (2021), e00664.
[16] H.M. Saleh, S.B. Eskander, Impact of water flooding on hard cement-recycled polystyrene composite immobilizing radioactive sulfate waste simulate, Constr. Build. Mater 222 (2019) 522–530.
[17] H.M. Saleh, F.A. El-Saied, T.A. Salaheldin, A.A. Hezo, Influence of severe climatic variability on the structural, mechanical and chemical stability of cement kiln dust-slag-nanosilica composite used for radwaste solidification, Constr. Build. Mater 218 (2019) 556–567, https://doi.org/10.1016/j.conbuildmat.2019.05.145.
[18] A. Mehta, D.K. Ashish, Silica fume and waste glass in cement concrete production: a review, J. Build. Eng. 29 (2020) 100888, https://doi.org/10.1016/j.jobe.2019.100888.
[19] M. Adaway, Y. Wang, Recycled glass as a partial replacement for fine aggregate in structural concrete–Effects on compressive strength, Electron. J. Struct. Eng. 14 (2015) 116–122.
[20] F. Krausmann, S. Gingrich, N. Eisenmenger, K.-H. Erb, H. Haberl, M. Fischer-Kowalski, Growth in global materials use, GDP and population during the 20th century, Ecol. Econ. 68 (2009) 2696–2705.
[21] A. Saccani, M.C. Bignozzi, ASR expansion behavior of recycled glass fine aggregates in concrete, Cem. Concr. Res. 40 (2010) 531–536.
[22] N.A. Soliman, A.F. Omran, A. Tagnit-Hamou, Laboratory characterization and field application of novel ultra-high-performance glass concrete, ACI Mater. J. 113 (2016) 307.
[23] A. Omran, A. Tagnit-Hamou, Performance of glass-powder concrete in field applications, Construct. Build. Mater. 109 (2016) 84–95.
[24] A.S. For T. and M.C.C.-1 on Cement, Standard Test Method for Compressive Strength of Hydraulic Cement Mortars (Using 2-in. or [50-mm] Cube Specimens), ASTM International, 2013.
[25] A. Standard, Standard Test Methods for Apparent Porosity, Water Absorption, Apparent Specific Gravity, and Bulk Density of Burned Refractory Brick and Shapes by Boiling Water, ASTM C20-00, West Conshohocken, PA, 2015.
[26] H.M. Saleh, I.I. Bondouk, E. Salama, H.A. Esawii, Consistency and shielding efficiency of cement-bitumen composite for use as gamma-radiation shielding material, Prog. Nucl. Energy 137 (2021) 103764.
[27] M.I. Abbas, M. Elsafi, M.M. Gouda, M. Abd-Elzaher, A. Hamzawy, M.S. Badawi, A.A. Thabet, S. Noureddine, A.M. El-Khatib, NaI cubic detector full-energy peak efficiency, including coincidence and self-absorption corrections for rectangular sources using analytical method, J. Radioanal. Nucl. Chem. 327 (2021) 251–258.
[28] M.S. Badawi, S. Noureddine, Y.N. Kopatch, M.I. Abbas, I.N. Ruskov, D.N. Grozdanov, A.A. Thabet, N.A. Fedorov, M.M. Gouda, C. Hramco, Characterization of the efficiency of a cubic NaI detector with rectangular cavity for axially positioned sources, J. Instrum. 15 (2020) P02013.
[29] G.A. Alharshan, D.A. Aloraini, M.A. Elzaher, M.S. Badawi, M.T. Alabsy, M.I. Abbas, A.M. El-Khatib, A comparative study between nano-cadmium oxide and lead oxide reinforced in high density polyethylene as gamma rays shielding composites, Nucl. Technol. Radiat. Protect. 35 (2020) 42–49, https://doi.org/10.2298/NTRP2001042A.
[30] M.A. Kiani, S.J. Ahmadi, M. Outokesh, R. Adeli, H. Kiani, Study on physico-mechanical and gamma-ray shielding characteristics of new ternary nano-composites, Appl. Radiat. Isot. 143 (2019) 141–148.
[31] M.I. Sayyed, M.G. Dong, H.O. Tekin, G. Lakshminarayana, M.A. Mahdi, Comparative investigations of gamma and neutron radiation shielding parameters for different borate and tellurite glass systems using WinXCom program and MCNPX code, Mater. Chem. Phys. 215 (2018) 183–202.
[32] J.F. Briesmeister, MCNP^< TM>-A General Monte Carlo N-Particle Transport Code, Version 4C, LA-13709-M, 2000.
[33] S. Hurtado, M. Garcıa-León, R. Garcıa-Tenorio, GEANT4 code for simulation of a germanium gamma-ray detector and its application to efficiency calibration, Nucl. Instruments Methods Phys. Res. Sect. A Accel. Spectrometers, Detect. Assoc. Equip. 518 (2004) 764–774.
[34] R. Brun, F. Rademakers, ROOT—an object oriented data analysis framework, Nucl. Instruments Methods Phys. Res. Sect. A Accel. Spectrometers, Detect. Assoc. Equip. 389 (1997) 81–86.
[35] M.I. Abbas, M.S. Badawi, A.A. Thabet, Y.N. Kopatch, I.N. Ruskov, D.N. Grozdanov, S. Noureddine, N.A. Fedorov, M.M. Gouda, C. Hramco, Efficiency of a cubic NaI (Tl) detector with rectangular cavity using standard radioactive point sources placed at non-axial position, Appl. Radiat. Isot. 163 (2020) 109139.
[36] M. Elsafi, M.A. El-Nahal, M.F. Alrashedi, O.I. Olarinoye, M.I. Sayyed, M.U. Khandaker, H. Osman, S. Alamri, M.I. Abbas, Shielding properties of some marble types: a comprehensive study of experimental and XCOM results, Materials 14 (2021) 4194, https://doi.org/10.3390/ma14154194.
[37] M.I. Sayyed, B. Albarzan, A.H. Almuqrin, A.M. El-Khatib, A. Kumar, D.I. Tishkevich, A.V. Trukhanov, M. Elsafi, Experimental and theoretical study of radiation shielding features of CaO-K_2O-Na_2O-P_2O_5 glass systems, Materials 14 (2021) 3772, https://doi.org/10.3390/ma14143772.
[38] Mengge Dong, Xiangxin Xue, Yang He, Zhefu Li, Highly cost-effective shielding composite made from vanadium slag and boron-rich slag and its properties, Radiat. Phys. Chem. 141 (2017) 239–244.
[39] S. Yasmin, B.S. Barua, Khandaker Mu, Rashid Ma, D.A. Bradley, Olatunji Ma, M. Kamal, Studies of ionizing radiation shielding effectiveness of silica-based commercial glasses used in Bangladeshi dwellings, Results Phys. 9 (2018) 541–549.
[40] S. Yasmin, Z.S. Rozaila, Khandaker Mu, B.S. Barua, F.U.Z. Chowdhury, Rashid Ma, D.A. Bradley, The radiation shielding offered by the commercial glass installed in Bangladeshi dwellings, Radiat. Eff. Defect Solid 173 (7–8) (2018) 657–672.
[41] M.I. Sayyed, O.I. Olarinoye, Elsafi Mohamed, Assessment of gamma-radiation attenuation characteristics of Bi2O3–B2O3–SiO2–Na2O glasses using Geant4 simulation code, Eur. Phys. J. Plus 136 (2021) 535, https://doi.org/10.1140/epjp/s13360-021-01492-y.